



# Underwater image dehazing using a novel color channel based dual transmission map estimation

Xiaohong Yan<sup>1,2</sup> · Guangyuan Wang<sup>1</sup> · Peng Lin<sup>1</sup> · Junbo Zhang<sup>1</sup> · Yafei Wang<sup>1</sup> · Xianping Fu<sup>1,3</sup>

Received: 14 January 2022 / Revised: 9 April 2022 / Accepted: 23 April 2023 /

Published online: 31 July 2023

© The Author(s), under exclusive licence to Springer Science+Business Media, LLC, part of Springer Nature 2023

## Abstract

Underwater images typically suffer from color distortion and low contrast, owing to the light absorption and scattering. To handle the visual manifestation of such degraded images, numerous underwater image dehazing algorithms have been presented. However, most of existing dehazing methods still have room for improvement in terms of preserving more details in the restored results. In this paper, we propose a simple yet effective dehazing method. The core idea is to produce the high-quality underwater images with rich detail information and vivid color. Firstly, an innovative color correction is designed to compensate the information of each color components. This operation is a pre-processing procedure, in which, selective absorption is fully considered. Then a dual transmission map-based haze removal method is introduced. Different from previous methods, a novel color channel with two terms is constructed to accurately estimate the transmission maps. The one is designed as the sharpened term to reveal more image detail and edges. The other is a difference of channel intensity prior term to remove the influence of light scattering. By using this strategy, our method can generate a natural appearance of the restored image with more detail information and higher color contrast. Experiments on representative images have proven that the performer of our method is 8.6% and 2.7% better than the second best on the average scores of patch-based contrast quality index (PCQI) and Entropy metrics, respectively.

**Keywords** Underwater image · Image dehazing · Color correction · Transmission map estimation

---

✉ Xianping Fu  
fxp@dlmu.edu.cn

Xiaohong Yan  
dl\_yanxiaohong@163.com

<sup>1</sup> Information Science and Technology School, Dalian Maritime University, Dalian 116026, China

<sup>2</sup> School of Software, Dalian Jiaotong University, Dalian 116028, China

<sup>3</sup> Pengcheng Laboratory, Shenzhen, Guangdong 518055, China

## 1 Introduction

Images acquired in harsh underwater scenes are usually characterized by insufficient visibility due to light attenuation (i.e., absorption and scattering). The absorption leads to color distortion such as greenish and bluish, depending on wavelength and scene-depth. Scattering changes the direction of light propagation, resulting in low contrast and blurry images. Such degraded images do not perform well in fundamental computer vision-based tasks, e.g. detection [21, 43], compression [58], segmentation [25, 51], and adaptive tracking control [29, 30]. To this end, there is an urgent need for dehazing techniques to improve the visual quality of underwater images. But, it is challenging owing to the medium attenuation properties and complex illumination.

To deal with these issues, a series of methods based on image formation model (IFM) [10, 36] have been introduced. Mathematically, the simplified IFM can be defined as:

$$I_c(x) = J_c(x)t_c(x) + B_c(1 - t_c(x)), c \in \{r, g, b\} \quad (1)$$

where  $I_c(x)$  is the observed intensity in color channel  $c$  at pixel  $x$ ,  $J_c(x)$  is the scene radiance,  $B_c$  is the background light (BL),  $t_c(x)$  is the transmission map (TM). In the (1), the TM represents portion of the scene radiance that is not absorbed and scattered. Broadly speaking, the TM implicitly reflects the degradation degrees of underwater images.

To estimate the derived parameters (BL and TM) described in (1), He et al. [18] firstly proposed the dark channel prior (DCP). This work has motivated various image dehazing methods [5] that modify the DCP [18] for underwater scenario. Instead of using the DCP, there are also useful priors proposed by other single image dehazing techniques. For example, Carlevaris-bianco et al. [4] designed a maximum intensity prior (MIP) to estimate the depth of scene. The MIP method exploits the large difference in attenuation among R-G-B color channels of an underwater image. Zhu et al. [62] proposed a color attenuation prior to restore the scene radiance of hazy image. Despite the valuable achievements achieved by these methods, they still introduce several disadvantages:

- (1) Traditional underwater image dehazing methods rarely take into account the wavelength- and scenedepth- dependent absorption, i.e., selective absorption. However, the absorption in the natural water generally plays a crucial role [1, 12].
- (2) Most methods [57, 60] apply post-processing steps to improve the image detail information. It can achieve a comparable performance, but this strategy may disrupt structure of the target input, and produce unnatural results.

To solve the above mentioned problems, we propose a novel haze removal method. Firstly, an innovative color correction technique is presented as a pre-processing procedure to compensate the attenuation of R-G-B color components. Secondly, we calculate the global background light from a local region of the color corrected image. Thirdly, a dual transmission map-based haze removal technique is introduced. Finally, the restored image is calculated with inversion of the simplified IFM. The proposed method can effectively remove the color distortion and improve the details, as shown in Fig. 1. It can be seen, the dehazed image obtains more number of visible edges than the original image. Put differently, the effectiveness of the proposed method can be further demonstrated by the application of visual edge detection [17]. Overall, the specific contributions can be summarized as follows:

- We propose a new restoration method to overcome the problem of underwater image degradation. Color correction is first utilized to establish the foundation for next dehazing step. Here, a novel technique is presented to remove the hazy based on dual transmission



**Fig. 1** Example of dehazed underwater image yielded by the proposed method. (a) Original image, (b) the edge map of (a), (c) dehazed image, (d) the edge map of (c). The values in represent the number of visible edges (VE) [17]

map estimation. Experimental results demonstrate that the proposed method can effectively remove the color distortion, and enhance the visual detail information (See Fig. 1).

- We propose a novel color correction method to eliminate the color distortion of real-world underwater images. Our method considers the selective light absorption that has not been taken seriously in the most existing techniques. Gain components are introduced to compensate the light attenuation by calculating the differences between the reference color channel and the degraded channels.
- To remove the haze performance of underwater images, a novel color channel based dual transmission map estimation method is proposed. Here, two terms are formulated to model this channel. For the first time, a detail sharpened term is introduced to effectively improve the deterioration of image edges. The other is designed as a difference of channel intensity prior term to mitigate the influence of light scattering. With the power of this channel, more detail information will be unveiled in the restored images.

The remainder of this paper is organized as follows: Section 2 introduces the work related to underwater dehazing. The proposed method is described in Section 3. Section 4 evaluates and compares experimental results. Section 5 concludes the paper.

## 2 Related work

There are two groups of image dehazing methods: learning-based methods [28, 32] and traditional methods [44, 53]. Generally, the traditional methods can be further categorized into underwater image enhancement methods [15] and underwater image restoration methods [34].

### 2.1 Learning-based method

With the popularity of Graphics Processing Unit (GPU), the deep learning approaches [41, 48, 49] have become the most advanced solution. These learning-based methods make a great performance in the computer vision fields. For example, Li et al. [24] synthesized underwater images from in-air color images by an unsupervised pipeline. These images served as inputs to a two-stage strategy to remove the color distortion. Fabbri et al. [9] designed an underwater generative adversarial network (UGAN) to improve the visual quality of underwater scenes. This method used cycle generative adversarial network (CycleGAN) [61] as a pre-processing step to obtain synthetic underwater images. Islam et al. [35] introduced a fully-convolutional conditional GAN-based model for real-time underwater image enhancement, called FUN-

IEGAN. Its training data was generated via the same strategy proposed by Fabbri et al. [61]. Recently, Guo et al. [16] presented a multiscale dense generative adversarial network (DenseGAN). It applied the dense connections, residual learning, and multi-scales network to facilitate the performance of underwater images enhancement. Li et al. [28] proposed an underwater image enhancement convolutional neural network method based on underwater image prior, named UWCNN. In 2021, with the medium transmission map guiding, Li et al. [27] proposed a deep learning-based model. This method fused the key features of the raw image in different color spaces to improve the quality of underwater images.

## 2.2 Underwater image enhancement method

In the last years, various image enhancement methods have been proposed to obtain a haze-free underwater image. For example, Fu et al. [13] introduced a retinex-based method to enhance underwater image. Zhang et al. [47] proposed an extended multi-scale retinex-based model. In CIEL<sup>a\*b\*</sup> color space, the bilateral and trilateral filter were used. Ancuti et al. [2] compensated for the attenuation via blending multiple images derived from color corrected image in the fusion strategy. Zhuang et al. [63] integrated gradient domain guided image filtering priors into a retinex-based technique. Recently, Zhang et al. [59] applied bi-interval histogram and s-shaped function on the degraded underwater images. Ding et al. [6] proposed a scene depth regularized method to enhance the underwater images. Ulutas et al. [45] firstly used the global contrast enhancement and the local technique to generate the dehazed images. Then color compensation was used to obtain the final results.

## 2.3 Underwater image restoration method

Most underwater image restoration methods are based on the IFM [10, 36], and calculate the derived parameters (background light or BL and transmission map or TM). Without additional information, BL and TM are difficult to estimate. Thus, dark channel prior (DCP) [18] was introduced to remove haze. For a target input  $I_c$ , DCP can be defined as:

$$I_{rgb}^{dark}(x) = \min_{y \in \Omega(x)} \left\{ \min_c I_c(y) \right\} \quad (2)$$

where  $\Omega(x)$  means a local patch centered at  $x$ . To calculate BL, the top 0.1 % brightest pixels were selected from  $I_{rgb}^{dark}$ . Then those bright values were mapped to  $I_c$ , and the highest intensity pixel can be estimated as BL.

In order to estimate TM, dividing both sides of (1) by BL, i.e.,  $B_c$  and then applying minimum operation on it, that is:

$$\min_{y \in \Omega(x)} \left\{ \min_c \frac{I_c(y)}{B_c} \right\} = t_c(x) \min_{y \in \Omega(x)} \left\{ \min_c \frac{J_c(y)}{B_c} \right\} + 1 - t_c(x) \quad (3)$$

For a haze-free image,  $J_{rgb}^{dark}$  is generally close to 0, that is:

$$J_{rgb}^{dark}(x) = \min_{y \in \Omega(x)} \left\{ \min_c J_c(y) \right\} = 0 \quad (4)$$

Putting (4) into (3), TM can be derived as:

$$t_c(x) = 1 - \min_{y \in \Omega(x)} \left\{ \min_c \frac{I_c(y)}{B_c} \right\} \quad (5)$$

To preserve the naturalness of image, a small amount of haze are retained in the restored underwater image  $J_c$ . Therefore, (5) can be rewritten as:

$$t_c(x) = 1 - \omega \min_{y \in \Omega(x)} \left\{ \min_c \frac{I_c(y)}{B_c} \right\} \quad (6)$$

Finally, with the estimated  $B_c$  and  $t_c(x)$ , the scene radiance is defined as:

$$J_c(x) = \frac{I_c(x) - B_c}{\max(t_c(x), t_0)} + B_c \quad (7)$$

where  $t_0$  is used to increase the exposure of the  $J_c$ .

There are many methods [20] based on DCP. For example, Drews Jr et al. [7] applied the DCP in the green and blue channels to estimate the transmission for underwater scenes. Galdran et al. [14] creatively developed a red channel prior (RCP) to restore the underwater images. This method took into account the colors associated to short wavelengths, i.e., red channel. Li et al. [23] introduced an underwater image dehazing algorithm based on the minimum information loss principle and histogram distribution prior. Wang et al. [50] proposed an adaptive attenuation-curve prior for underwater image dehazing. Peng et al. [38] presented a generalized dark channel prior (GDCP) for restoring degraded underwater images. Song et al. [42] proposed a scene depth estimation model based on underwater light attenuation prior (ULAP). This method applied learning-based supervised linear regression to train the model. Recently, Yu et al. [57] presented an effective pipeline to enhance underwater images. In this method, homomorphic filtering, double transmission map, and dual-image wavelet fusion were used.

These methods have made remarkable success in the image dehazing field. However, there are still some defects in the estimation of TM, which cause their results to be unnatural. In order to address these issues, we propose an effective underwater image dehazing method, which will be described in detail in Section 3.

### 3 Proposed method

In this section, the goal of the proposed method is to generate a haze-free underwater image with good visibility. The framework of the proposed method is shown in Fig. 2.

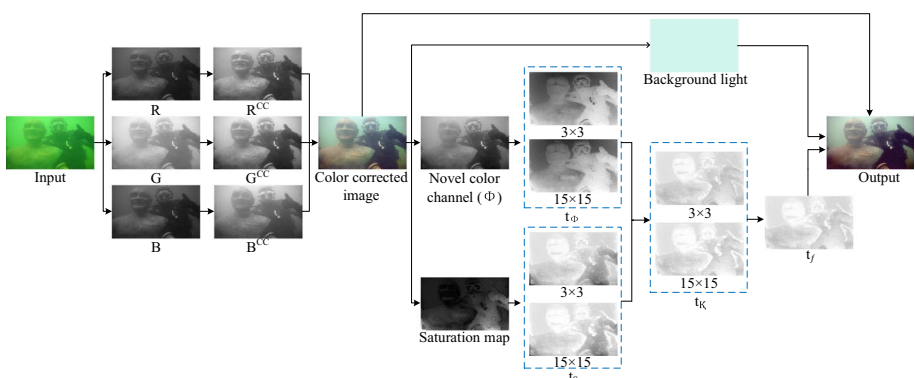


**Fig. 2** The framework of the proposed method

### 3.1 Color correction

Due to complex light source or medium attenuation properties, underwater images are usually characterized by color distortion. For example, in Fig. 3 (a), the red channel with the longest wavelength is attenuated faster than blue and green ones, the blue channel is well preserved (see Fig. 3 (b)). In contrast, for Fig. 3 (c), the blue channel with the shortest wavelength may also be attenuated, owing to the absorption of organic matter in sea water. The green channel is relatively well preserved compared with the red and blue ones (see Fig. 3 (d)). To alleviate some of the color distortion, several traditional color correction techniques based on linear stretching are proposed. However, most of these methods do not work well (see Fig. 4 and 5), due to not fully considering the unbalanced attenuation caused by selective absorption. To solve the issues mentioned above, in this paper, an effective color correction method is proposed.

For an underwater image  $I_c$ ,  $c \in \{r, g, b\}$ , we first estimate a reference map  $I_\theta(x)$  with well-preserved information. Here,  $I_\theta(x) = \max(I_c(x))$ . Then, in order to adaptively compensate for the loss of the degraded channels, a gain component  $g_c(x)$  is proposed, which can be defined as:

$$g_c(x) = (1 - \bar{I}_c) \left( \frac{I_\theta(x) - I_c(x)}{I_c(x)} \right)^\beta \quad (8)$$

where  $\bar{I}_c$  is the mean value of color component  $I_c$ ,  $\beta$  is set as 0.7. Finally, a linear operation is used for each color channel as follows:

$$I_c^{CC}(x) = \frac{I_c(x) \times (1 + g_c(x)) - I_c^{\min}}{I_c^{\max} - I_c^{\min}} \quad (9)$$

where  $I_c^{CC}$  means the color corrected image.

Figure 4 shows the comparisons of several well-known color correction methods. It can be observed that the proposed color correction method achieves a more appropriate color. The Grey Edge [52], Max RGB [22], and Grey pixel [55] are not able to entirely remove color distortion. The Shades of Grey [11], Grey World [3] and color constancy [54] methods show better results, but often tend to produce a reddish images.

Since the color is often taken differently through different cameras. Figure 5 shows the comparisons of several methods to further examine the color corrected accuracy of images taken at different camera settings. The cameras used to capture the underwater images are Canon D10, FujiFilm Z33, Olympus Tough 6000, and Pentax W60. The four images have been taken about 1 meter away from the object. The cameras are set to maximum zoom setting, apart from the Pentax W60, which is set close to 35 mm. CIEDE2000 [40] is employed to evaluate the color difference between the reference ground truth Macbeth Color Checker and the corresponding color patch, manually located in each image. From Table 1, it can be seen, the proposed color correction method as a pre-processing step shows the lowest value than other methods in most of cases.

Figure 6 shows the results yielded by the proposed color correction method with different  $\beta$ . It can be seen, when  $\beta$  is set as 0.4, the method will not able to entirely remove color casts. When  $\beta$  is set as 1, the color corrected image will be over-compensated. So, in the following experiments,  $\beta$  is set as 0.7.

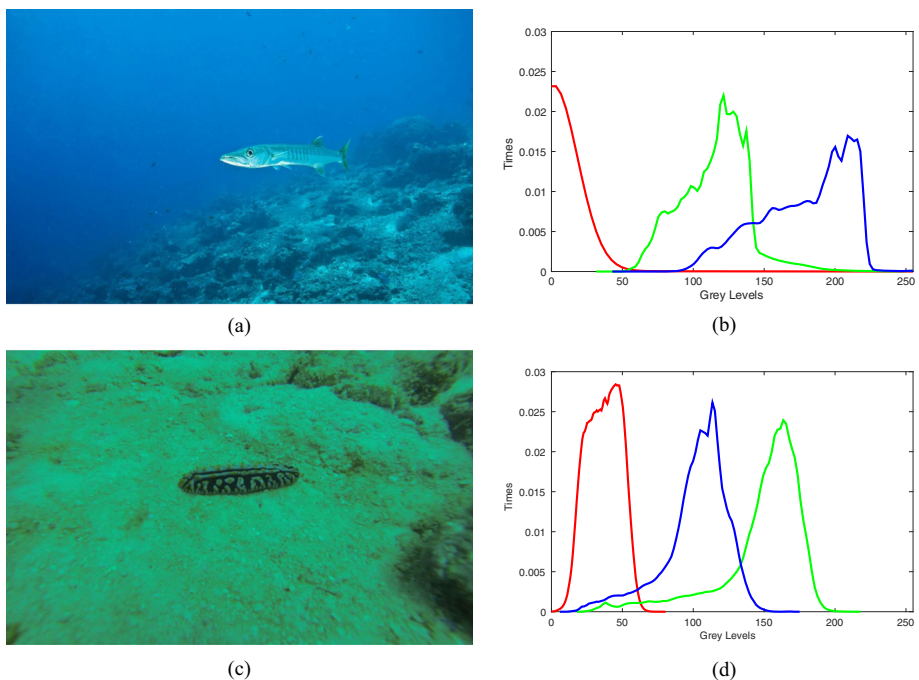


**Fig. 3** Examples of underwater image. (a) and (c) Original underwater images, (b) and (d) represents the histogram distributions of (a) and (c), respectively

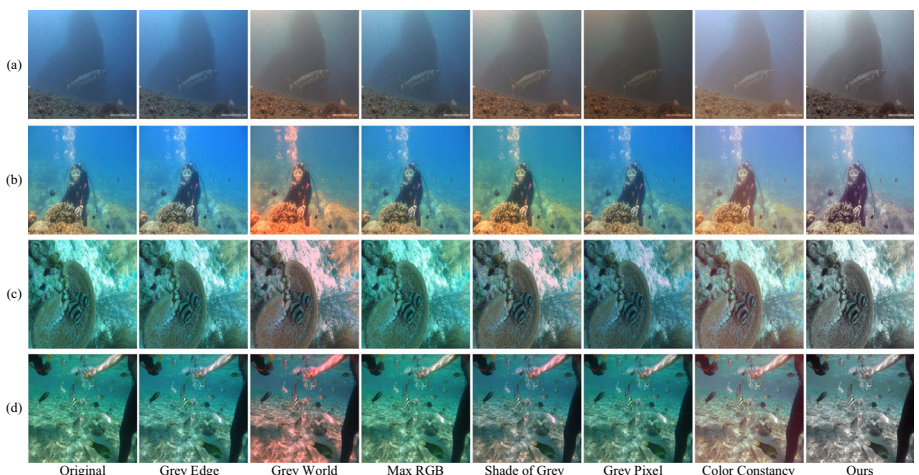


**Fig. 4** Comparisons of several color correction methods (Grey Edge [52], Grey World [3], Max RGB [22], Shades of Grey [11], Grey Pixel [55], and Color Constancy [54])

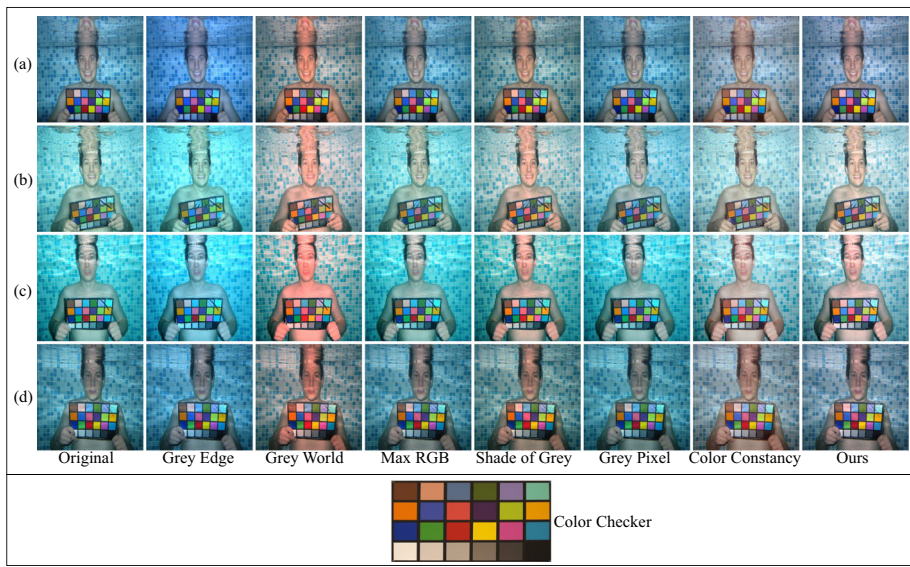


**Fig. 5** Comparisons of several color correction methods (Grey Edge [52], Grey World [3], Max RGB [22], Shades of Grey [11], Grey Pixel [55], and Color Constancy [54]). The color checker is used as a reference for calculating CIEDE2000 [40]. The range of CIEDE2000 is [0, 100], a smaller value indicates a small color difference. In other words, the smaller the metric, the better. The quantitative results are provided in Table. 1

### 3.2 Underwater image dehazing

The proposed color correction procedure described in Section 3.1 can eliminate color distortion to some extent. However, the color corrected image still shows the appearance of low visibility caused by light scattering (See Fig. 7). In this section, we propose an effective restoration method to generate haze-free underwater images from the color corrected versions.

#### 3.2.1 Background light

By referring to (1), the color corrected underwater image  $I_c^{CC}$  can be represented as:

$$I_c^{CC}(x) = J_c(x)t_c(x) + B_c(1 - t_c(x)) \quad (10)$$

**Table 1** Quantitative evaluation of color correction based on CIEDE2000 [40] measure

Image	CIEDE2000						
	Grey Edge	Grey World	Max RGB	Shades of Grey	Grey Pixel	Color Constancy	Ours
Figure 5 (a)	24.38	10.77	18.86	<b>10.71</b>	18.89	10.91	<b>9.60</b>
Figure 5 (b)	26.86	<b>10.84</b>	20.32	13.33	20.98	12.49	<b>11.37</b>
Figure 5 (c)	26.05	13.69	21.81	15.05	21.71	<b>12.92</b>	<b>11.53</b>
Figure 5 (d)	20.98	<b>11.37</b>	16.41	11.88	18.93	11.65	<b>10.80</b>

The corresponding images (same order) are presented in Fig. 5. First and second best results are highlighted in color

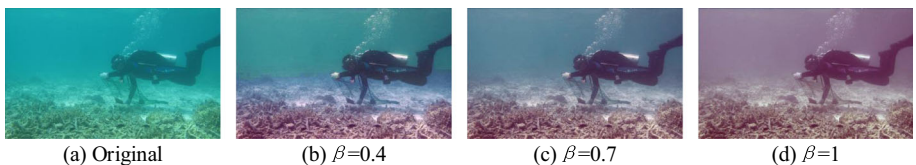


**Fig. 6** The effect of the parameter  $\beta$ . (a) Original image, (b)-(d) respectively represent the color corrected images with third different values of  $\beta$ . Setting  $\beta = 0.7$  practically results in the most satisfactory images

It is evident from Section 2.3 (especially (2)-(5)) that the existing DCP-based techniques used a global strategy to estimate the BL or  $B_c$ . When considering the underwater image, these techniques show limitations due to the existence of various light sources. Thus, we estimate the BL from local region. Similar to [39], the color corrected image  $I_c^{CC}$  is divided into  $N$  blocks of  $32 \times 32$  size. To estimate a smooth background block, the score of each block is calculated as the average pixel value subtracted by the standard deviation of the pixel values within the block. The candidate block is obtained by seeking the block with highest score. The top 5% brightest pixels in the dark channel of the candidate block is selected to alleviate the effect of floating particles. Moreover, the selected pixels are mapped to the color corrected image. Finally the mean value of the selected pixels is calculated, which considered as the background light  $B_c$ . Figure 8 shows two examples of the proposed BL estimation method. It can be seen that our method can effectively calculate the BL from the color corrected images.

### 3.2.2 Transmission map

After calculating the  $B_c$ , the visual quality of the dehazed underwater images usually relies on the estimation of the TM. In view of the similarities between outdoor terrestrial images and real-world underwater images, we use the DCP [18] to estimate the TM. By referring to (6), the TM, i.e.,  $t_c(x)$  is rewritten as:

$$t_c(x) = 1 - \omega \min_{y \in \Omega(x)} \left\{ \min_c \frac{I_c^{CC}(y)}{B_c} \right\} \quad (11)$$

where  $c \in \{r, g, b\}$ ,  $\omega$  is used to maintain a small amount of haze in the restored image, it is empirically set to 0.85. Interestingly, the TM estimated via (11) is not always correct.

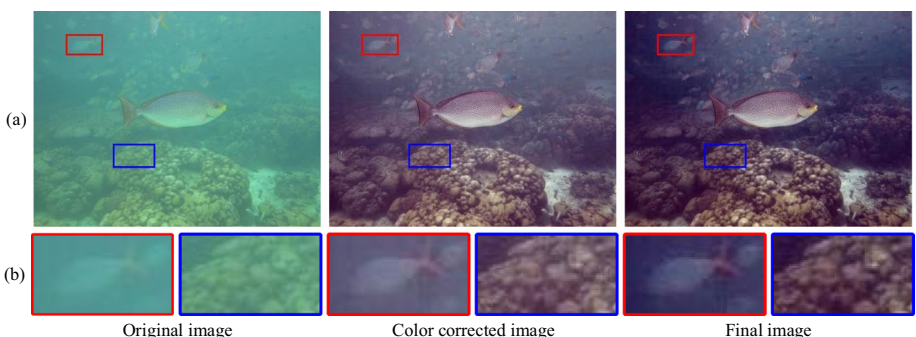


**Fig. 7** Example of color corrected image and final restored image



**Fig. 8** Examples of BL estimation. (a) Color corrected image, (b) background light

Inspired by [39], we design a novel color channel  $\phi(x)$  to estimate the TM, which is defined as:

$$\phi(x) = L(x) + (L(x) - G(x) * L(x)) - \delta \quad (12)$$

where  $L(x) = 0.299I_r^{CC}(x) + 0.587I_g^{CC}(x) + 0.114I_b^{CC}(x)$ ,  $\delta = \max(I_c^{CC}(x)) - \min(I_c^{CC}(x))$ ,  $G(x)$  means a two-dimensional Gaussian function with  $\sigma = 0.5$  and a size of  $8 \times 8$  pixels, and  $*$  denotes a convolution operator.

Here, we explain the motivation behind (12) as follows. Since removing the haze from a single image is at the cost of losing detail. Thus,  $L(x) + (L(x) - G(x) * L(x))$  is firstly used as the sharpened term to compensated for this loss. What's more, in the background region of an image is inhomogeneous owing to the difference in light scattering angles.  $\delta$  is used as a difference of channel intensity prior term to eliminating the influence of light scattering. Thus, referring to (11), TM is derived as:

$$t_\phi(x) = 1 - \omega \min_{y \in \Omega(x)} \left\{ \min_c \frac{\phi(y)}{B_c} \right\} \quad (13)$$

where  $\Omega(x)$  means a local patch centered at  $x$ . To generate natural haze-free underwater images, we apply  $3 \times 3$  and  $15 \times 15$  for smaller and larger patch size, respectively. In other words, dual TMs, i.e.,  $t_{\phi_{3 \times 3}}(x)$  and  $t_{\phi_{15 \times 15}}(x)$  are estimated from (13). Furthermore, we present a saturation map  $S(x)$ , which can be defined as:

$$S(x) = \frac{\max_{y \in \Omega} I_c^{CC}(y) - \min_{y \in \Omega} I_c^{CC}(y)}{\max_{y \in \Omega} I_c^{CC}(y)} \quad (14)$$

where  $S(x)$  is used to mitigate the effect of bright element, e.g., artificial light (AL). In the HSV color model, the dark regions of the underwater image often appear fully saturated. On the contrary, the lack of saturation in an area will be interpreted as a lot of white light shooting. Thus, to express the above observation, a lower-bound TM, i.e.,  $t_S(x)$  can be readily available from (15) as:

$$t_S(x) = 1 - S(x) \quad (15)$$

where  $t_S(x)$  means  $t_{S_{3 \times 3}}(x)$  and  $t_{S_{15 \times 15}}(x)$ . After this, dual rough TMs, i.e.,  $t_{\kappa_{3 \times 3}}(x)$  and  $t_{\kappa_{15 \times 15}}(x)$  are obtained by:

$$t_{\kappa_{3 \times 3}}(x) = \max(t_{\phi_{3 \times 3}}(x), t_{S_{3 \times 3}}(x)) \quad (16)$$

$$t_{k_{15 \times 15}}(x) = \max(t_{\phi_{15 \times 15}}(x), t_{S_{15 \times 15}}(x)) \quad (17)$$

So, according to (16) and (17),  $t_{\kappa'}(x)$  is defined as:

$$t_{\kappa'}(x) = \lambda(x) \times t_{k_{3 \times 3}}(x) + (1 - \lambda(x)) \times t_{k_{15 \times 15}}(x) \quad (18)$$

where

$$\lambda(x) = \frac{t_{k_{3 \times 3}}(x) - t_{k_{15 \times 15}}(x)}{t_{k_{15 \times 15}}(x) + \epsilon} \quad (19)$$

where  $\epsilon$  is an infinitesimal to prevent division by zero.

Since the TM is deduced through a local patch of the image, some undesired artifacts will appear in the process. To settle this issue, the guided filter [19] is further employed to obtain the refined TM, i.e.,  $t_f(x)$ .

### 3.2.3 Radiance

At last, the restored image  $J_c(x)$  is calculated by using the background light  $B_c$  and the refined transmission map  $t_f(x)$ . By referring to (7),  $J_c(x)$  is defined as:

$$J_c(x) = \frac{I_c^{CC}(x) - B_c}{\max\{t_f(x), t_0\}} + B_c \quad (20)$$

where  $t_0$  is taken as 0.1 to avoid the denominator is zero. For clarity, the detailed steps of the proposed method are outlined in Algorithm 1.

---

#### Algorithm 1 Overall algorithm of the proposed method.

---

**Input:** underwater image  $I_c$

**Output:** restored image  $J_c$

- 1: estimate the reference map  $I_\theta(x)$  using  $I_\theta(x) = \max(I_c(x))$ .
  - 2: calculate the gain component  $g_c(x)$  using (8).
  - 3: obtain the color corrected image  $I_c^{CC}(x)$  using (9).
  - 4: divide  $I_c^{CC}(x)$  into  $N$  blocks of  $32 \times 32$  size.
  - 5: calculate the score of each block using the average pixel value subtracted by the standard deviation of the pixel values within the block.
  - 6: seek a block with highest score as the candidate block.
  - 7: select the top 5% brightest pixels in the dark channel of the candidate block.
  - 8: calculate the mean value of the selected pixels as the  $B_c$ .
  - 9: calculate the novel color channel  $\phi(x)$  using (12).
  - 10: estimate the saturation map  $S(x)$  using (14).
  - 11: obtain the  $t_\phi(x)$  (i.e.,  $t_{\phi_{3 \times 3}}(x)$  and  $t_{\phi_{15 \times 15}}(x)$ ) using (13).
  - 12: obtain the  $t_S(x)$  (i.e.,  $t_{S_{3 \times 3}}(x)$  and  $t_{S_{15 \times 15}}(x)$ ) using (15).
  - 13: obtain the  $t_{k_{3 \times 3}}(x)$  using (16).
  - 14: obtain the  $t_{k_{15 \times 15}}(x)$  using (17).
  - 15: obtain the  $t_{\kappa'}(x)$  using (18).
  - 16: obtain the  $t_f(x)$  using the guided filter.
  - 17: obtain the restored image  $J_c$  using (20).
- 

## 4 Experimental results and analysis

In this section, experiments are executed to examine the effectiveness of the proposed method. Test images are taken from the underwater image enhancement benchmark dataset (UIEBD)

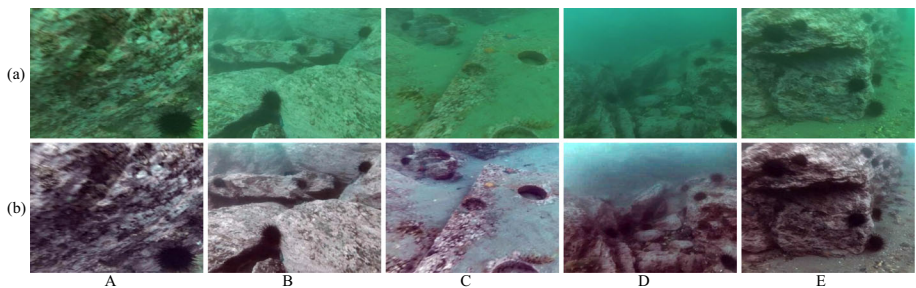


**Fig. 9** Dehazed results yielded by the proposed method. From left to right, original images from the five subsets A–E are ranked according to a non-reference underwater image quality evaluation (UCIQE) [56], and the corresponding image quality successively decreases [31]

[26] and underwater image quality set (UIQS) [31]. The UIEBD contains 890 real-world underwater images and 60 challenging data. The raw images in UIEBD are constructed from the Internet. These images have multiple color ranges and levels of contrast reduction. The underwater images in UIQS are captured by the authors in the First Underwater Robot Picking Contest, Zhangzidao, Dalian, China. We conduct comparative experiments with several underwater image enhancement/restoration methods, namely, DCP [18], GDPCP [38], MIP [4], RCP [7], FUNIEGAN [35], UGAN [8], ULAP [42], and UWCNN [28].

The proposed method is implemented in MATLAB R2020a using a PC with Intel Core(TM) i7-4710 CPU @ 2.50 GHz and 16 GB RAM.

#### 4.1 Evaluation of the proposed method

To evaluate the proposed method for the improvement of image visibility, we employ several underwater images. These test images are captured under shallow water at different quality levels. The corresponding dehazed results are shown in Fig. 9. It can be seen that the proposed

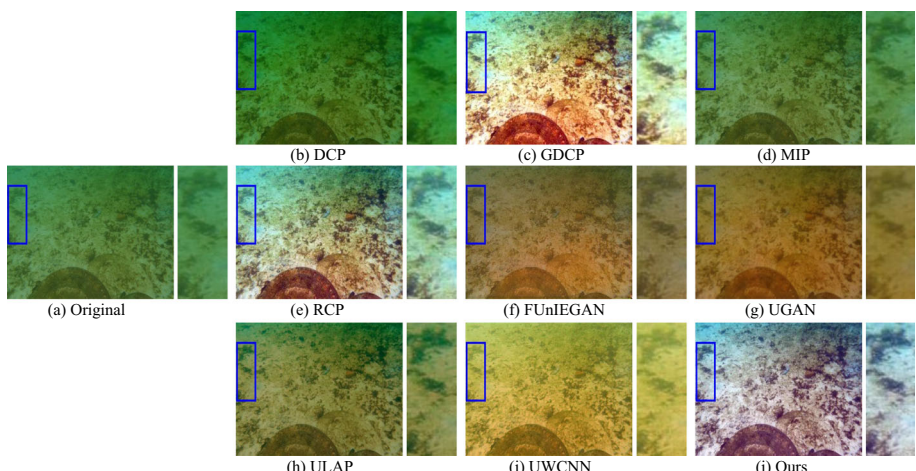


**Fig. 10** Qualitative comparisons of different methods. (a) Original image, (b) DCP, (c) GDCP, (d) MIP, (e) RCP, (f) FUNIEGAN, (g) UGAN, (h) ULAP, (i) UWCNN, (j) Ours

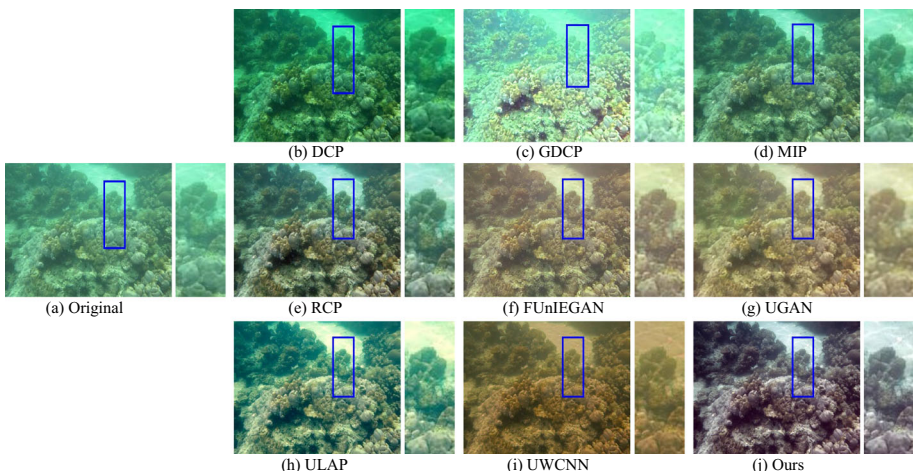


**Fig. 11** Qualitative comparisons of different methods. (a) Original image, (b) DCP, (c) GDCP, (d) MIP, (e) RCP, (f) FUNIEGAN, (g) UGAN, (h) ULAP, (i) UWCNN, (j) Ours

method is able to deal with images in various shallow water conditions. What's more, thanks to the novel color channel based dual transmission map estimation, the proposed method can clearly unveil the hidden details.

#### 4.2 Qualitative comparison

In the visual comparison, we select seven underwater images that were captured under different scenes (turbid scene and clear open scene). In turbid water, it contains more suspended particles and organic matter, which strongly absorb the shortest wavelength, resulting in yellowish or greenish appearance, as shown in Figs. 10, 11, 12, and 13. For these four images, the scene transmissions deduced via DCP [18] and MIP [4] are wrong, the restored images are similar to the raw. The GDCP [38] method fails to estimate transmission and calculate background light, leading to an unsatisfactory results. Although RCP [7] method can restore the image to a certain extent, it tends to show unnatural artifacts. The results obtained by ULAP [42] may introduce a color distortion appearance. The FUNIE-GAN [35], UGAN [8], and UWCNN [28] methods fail to improve contrast of an image and have poor effect on color correction.

In clear open water, visible light with the longest wavelength is absorbed at the highest rate, appearing green-bluish to the eye, as shown in Figs. 14, 15, and 16. Under clear open water, the restored images using DCP [18] method usually look darker, and possess a little color deviation. The results obtained by MIP [4] may introduce an unpleasing performance, owing to the inaccurate transmission map estimation. The dehazed images by GDCP [38] look brighter. The ULAP [42] method produces unsatisfying results with reddish color shift and artifacts. The FUNIE-GAN [35], UGAN [8], and UWCNN [28] cannot address this scene properly.

In summary, the proposed method successfully eliminates the effects of light attenuation. It introduces the high-quality underwater images with higher contrast and more detail information.

### 4.3 Quantitative comparison

Additionally, in order to quantitatively show the superiority of the proposed method, the quality of the restored underwater images is measured by using Entropy, patch-based contrast quality index (PCQI) [46], underwater image quality measures (UIQM) [37], and underwater color image quality evaluation (UCIQE) [56]. The Entropy is used for estimating the abundance of image information. Higher entropy values of an image reveal more information included in the image. PCQI method is used to deduce the human perception of contrast variations. A higher PCQI score, the better image contrast. PCQI is defined as:

$$PCQI = \frac{1}{M} \sum_{i=1}^M q_i(x_i, y_i) q_c(x_i, y_i) q_s(x_i, y_i) \quad (21)$$

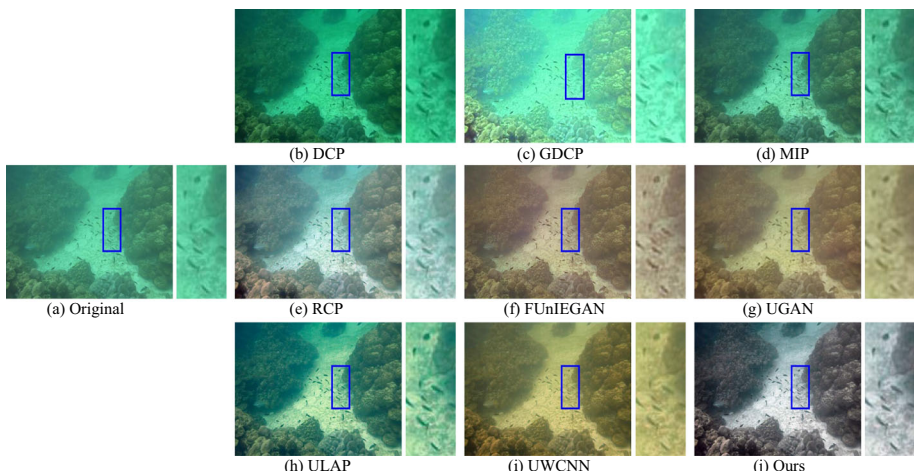


**Fig. 12** Qualitative comparisons of different methods. (a) Original image, (b) DCP, (c) GDCP, (d) MIP, (e) RCP, (f) FUNIEGAN, (g) UGAN, (h) ULAP, (i) UWCNN, (j) Ours

**Table 2** Underwater dehazing evaluation based on Entropy

Image	Fig. 10	Fig. 11	Fig. 12	Fig. 13	Fig. 14	Fig. 15	Fig. 16	Avg
DCP	7.072	7.499	7.459	7.058	7.631	7.530	6.819	7.295
GDCP	7.336	7.331	7.502	7.038	7.563	7.219	<b>7.357</b>	7.335
MIP	7.043	7.296	7.268	6.782	7.779	<b>7.633</b>	7.088	7.270
RCP	<b>7.601</b>	7.465	7.494	6.996	<b>7.808</b>	7.589	7.067	7.431
FUnIEGAN	7.218	7.067	6.966	6.531	7.604	7.527	7.343	7.179
UGAN	7.221	7.184	7.046	6.411	7.550	7.615	7.292	7.188
ULAP	7.159	<b>7.607</b>	<b>7.579</b>	<b>7.299</b>	7.648	7.552	7.232	<b>7.439</b>
UWCNN	7.588	7.224	7.314	6.997	7.046	6.734	7.246	7.164
Ours	<b>7.687</b>	<b>7.667</b>	<b>7.575</b>	<b>7.411</b>	<b>7.899</b>	<b>7.686</b>	<b>7.564</b>	<b>7.641</b>

First and second best results are highlighted in color

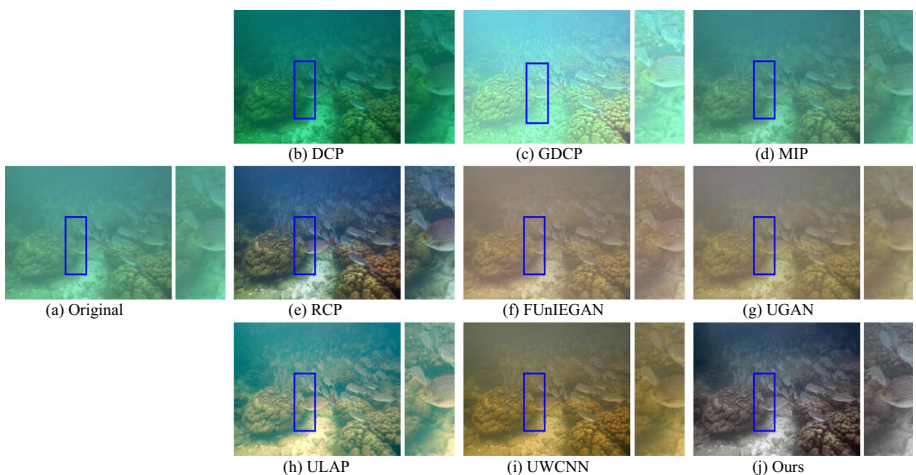


**Fig. 13** Qualitative comparisons of different methods. (a) Original image, (b) DCP, (c) GDCP, (d) MIP, (e) RCP, (f) FUNIEGAN, (g) UGAN, (h) ULAP, (i) UWCNN, (j) Ours

where  $M$  is the total number of the patches in the image,  $q_i$ ,  $q_c$  and  $q_s$  are three comparison functions.

The UIQM metric is designed specifically to quantify the colorfulness measure (UICM), sharpness measure (UISM), and contrast measure (UIConM) that characterize underwater images. UIQM is described as a linear combination:

$$UIQM = c_1 \times UICM + c_2 \times UISM + c_3 \times UIConM \quad (22)$$

where  $c_1$ ,  $c_2$ , and  $c_3$  mean the scale factors. According to the original work, we set  $c_1 = 0.0282$ ,  $c_2 = 0.0953$ , and  $c_3 = 3.5753$ .

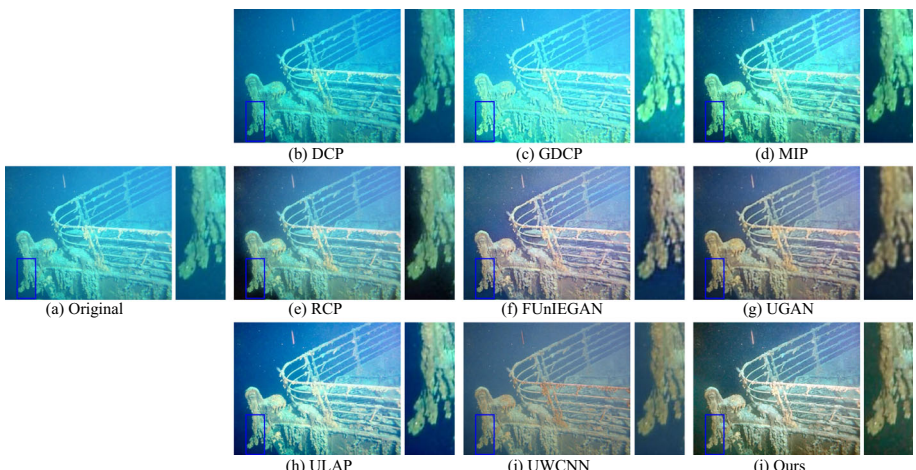


**Fig. 14** Qualitative comparisons of different methods. (a) Original image, (b) DCP, (c) GDCP, (d) MIP, (e) RCP, (f) FUNIEGAN, (g) UGAN, (h) ULAP, (i) UWCNN, (j) Ours

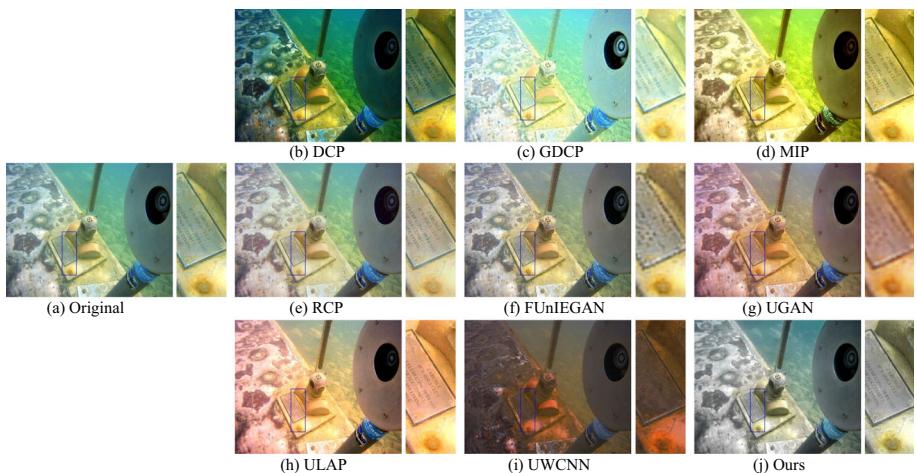


**Fig. 15** Qualitative comparisons of different methods. (a) Original image, (b) DCP, (c) GDCP, (d) MIP, (e) RCP, (f) FUNIEGAN, (g) UGAN, (h) ULAP, (i) UWCNN, (j) Ours

The UCIQE takes into account three underwater image quality criterions: chroma ( $\sigma_c$ ), saturation ( $con_l$ ) and contrast ( $\mu_s$ ). The UCIQE is defined as:

$$UCIQE = m_1 \times \sigma_c + m_2 \times con_l + m_3 \times \mu_s \quad (23)$$

where  $m_1$ ,  $m_2$  and  $m_3$  are the weighted coefficients. We use the recommended weighted coefficients ( $m_1 = 0.4680$ ,  $m_2 = 0.2745$ , and  $m_3 = 0.2576$ ). A greater value of the UIQM or UCIQE means better image quality.

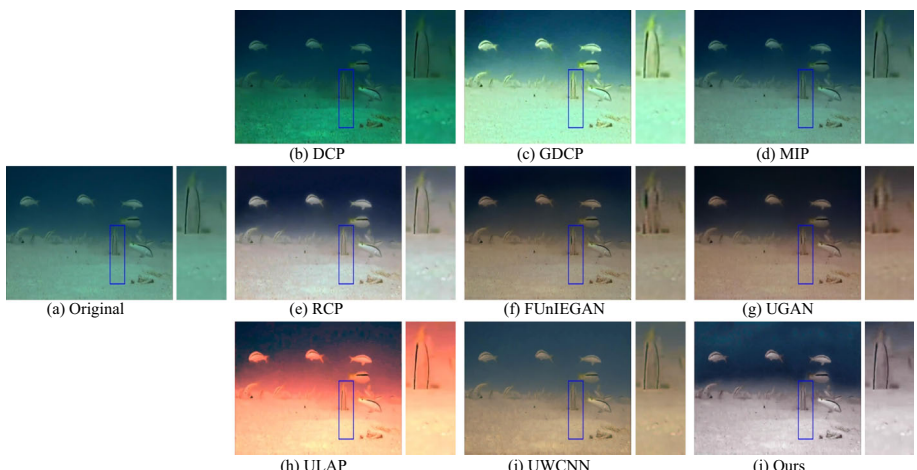


**Fig. 16** Qualitative comparisons of different methods. (a) Original image, (b) DCP, (c) GDCP, (d) MIP, (e) RCP, (f) FUNIEGAN, (g) UGAN, (h) ULAP, (i) UWCNN, (j) Ours

**Table 3** Underwater dehazing evaluation based on PCQI

Image	Fig. 10	Fig. 11	Fig. 12	Fig. 13	Fig. 14	Fig. 15	Fig. 16	Avg
DCP	0.987	0.917	0.937	0.897	0.937	0.834	0.882	0.913
GDCP	1.232	1.019	0.984	0.963	0.923	0.828	0.829	0.968
MIP	1.080	0.998	1.016	0.978	1.052	0.973	0.947	1.006
RCP	1.263	1.086	1.208	1.102	1.070	0.971	0.922	1.089
FUnIEGAN	0.859	0.857	0.905	0.899	0.843	0.496	0.897	0.822
UGAN	0.678	0.710	0.752	0.805	0.683	0.438	0.865	0.704
ULAP	1.191	1.170	1.166	1.224	1.093	0.950	0.817	1.087
UWCNN	1.031	0.869	1.062	1.038	0.844	0.591	0.915	0.907
Ours	1.305	1.168	1.277	1.349	1.116	0.981	1.083	1.183

**Table 4** Underwater dehazing evaluation based on UIQM

Image	Fig. 10	Fig. 11	Fig. 12	Fig. 13	Fig. 14	Fig. 15	Fig. 16	Avg
DCP	1.220	1.380	1.123	0.959	1.011	1.151	0.635	1.068
GDCP	1.553	1.368	1.089	0.938	0.993	0.976	0.641	1.080
MIP	1.166	1.258	1.015	0.743	1.117	1.007	0.567	0.982
RCP	1.478	1.464	1.325	1.133	1.112	0.858	0.723	1.156
FUnIEGAN	1.127	1.207	0.967	0.727	1.072	0.678	0.527	0.901
UGAN	0.920	1.036	0.786	0.626	0.967	0.603	0.533	0.782
ULAP	1.313	1.474	1.250	1.073	1.160	0.934	0.572	1.111
UWCNN	1.187	1.270	1.027	0.894	0.899	0.897	0.482	0.951
Ours	1.561	1.518	1.359	1.204	1.242	1.174	0.760	1.260

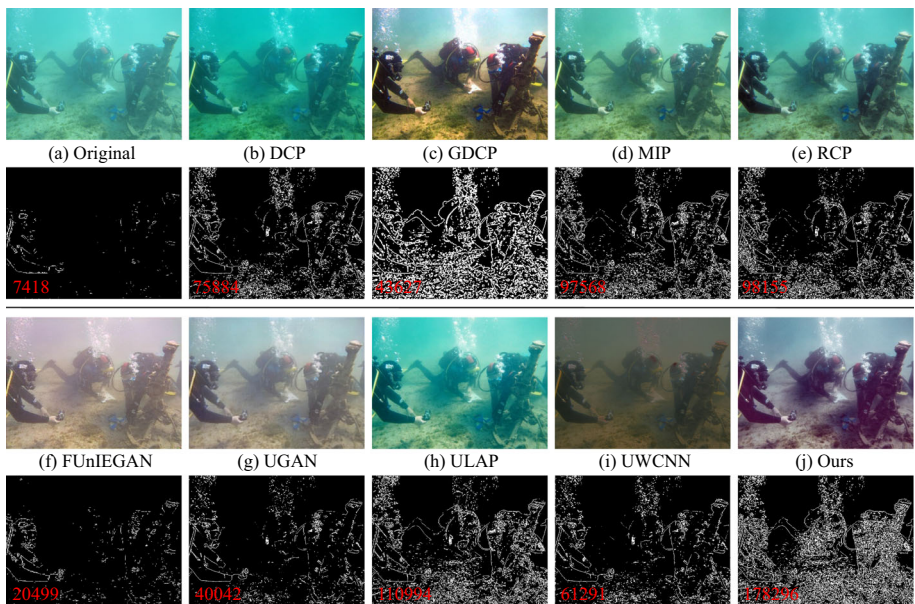
**Table 5** Underwater dehazing evaluation based on UCIQE

Image	Fig. 10	Fig. 11	Fig. 12	Fig. 13	Fig. 14	Fig. 15	Fig. 16	Avg
DCP	0.395	0.486	0.462	0.466	0.495	0.648	0.446	0.485
GDCP	0.599	0.479	0.412	0.399	0.441	0.604	0.541	0.496
MIP	0.405	0.473	0.459	0.421	0.549	0.610	0.469	0.484
RCP	0.565	0.569	0.581	0.552	0.581	0.578	0.555	0.569
FUnIEGAN	0.441	0.450	0.420	0.400	0.555	0.587	0.556	0.487
UGAN	0.422	0.461	0.435	0.422	0.569	0.598	0.553	0.494
ULAP	0.451	0.577	0.523	0.539	0.573	0.627	0.646	0.562
UWCNN	0.426	0.489	0.495	0.503	0.493	0.530	0.546	0.497
Ours	0.572	0.570	0.558	0.562	0.584	0.629	0.568	0.578

Tables 2, 3, 4, and 5 give the quantitative evaluations of the nine techniques for seven real-world underwater images selected in Section 4.2. We observe that output results of the proposed method are typically better than others in terms of Entropy, PCQI and UIQM. The best Entropy and PCQI values indicate that the proposed method can remarkably increase the meaningful detail information and improve the most of image contrast. The highest UIQM score means that the proposed method can effectively balance the colorfulness, sharpness, and contrast of the output images, and also produce most satisfactory results. It is well-known that UCIQE does not consider color casts and artifacts. To this end, from the UCIQE metric quality analysis of Table 5, the proposed method has slightly higher score than the related methods. The quantitative comparison further show the robustness and effectiveness of the proposed method.

#### 4.4 Verify the effectiveness of detail improvement

To fairly assess the effect of the proposed method, we also compare it with different methods through using the number of visible edges [17], as shown in Figs. 17 and 18. It can be



**Fig. 17** Experimental results about detail preserving among the images yielded by different methods. (a) Original image and it's visible edge maps. (b)-(j) the corresponding results of DCP, GDCP, MIP, RCP, FUnIEGAN, UGAN,ULAP, UWCNN, and Ours, respectively. The values in red represents the number of visible edges (VE) [17]

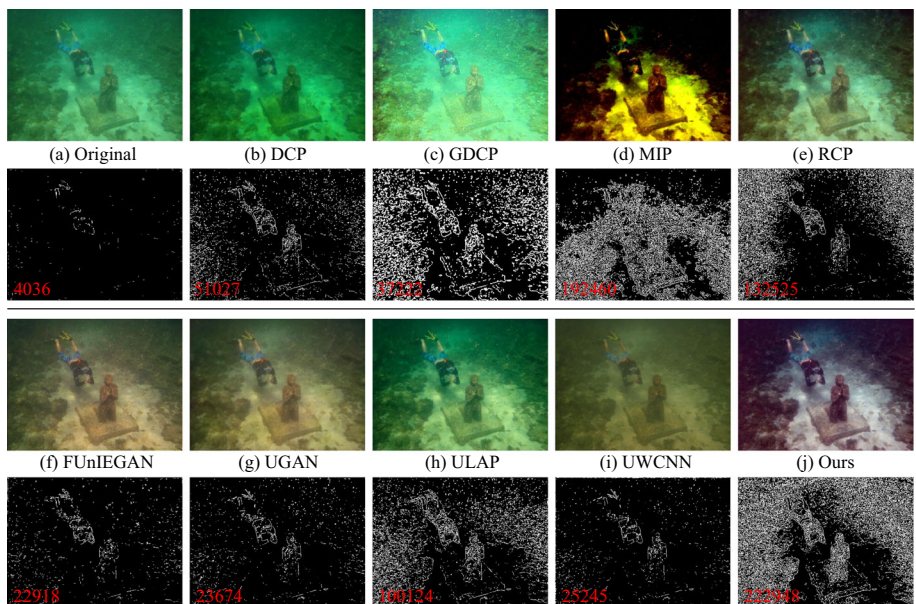


**Fig. 18** Experimental results about detail preserving among the images yielded by different methods. (a) Original image and it's visible edge maps. (b)–(j) the corresponding results of DCP, GDCP, MIP, RCP, FUNIEGAN, UGAN, ULAP, UWCNN, and Ours, respectively

observed that the edges of original underwater images are slightly detected, owing to the light scattering. For these underwater images, the previous techniques seem to introduce hazy in the restored results, which is reflected in the visible edge maps. Compared with the



**Fig. 19** Local feature point matching. (a) and (c) original underwater images, (b) and (d) our results



**Fig. 20** Other degraded images. (a) Original, (b) restored results yielded by the proposed method

original image, the number of the visible edges does not increase much. In contrast, the proposed method introduces more number of visible edges and effectively restores image details.

#### 4.5 Application test

We perform the local feature point matching to further examine the effectiveness of the proposed method. Here, scale invariant feature transform (SIFT) operator [33] is applied for keypoints calculation. Figure 19 shows the two examples of this application test. Each example includes a pair of underwater images, and the corresponding restored images generated through our method. For the top-side pair, the SIFT operator determine 3 valid matches on the raw underwater images, and 19 good matches for the restored underwater images obtained by our method. For bottom-side pair, SIFT extracts 2 good matches between the raw images. In contrast, it finds 34 valid matches for images restored via our method. The application test illustrates that our method introduces a good performance when it is used to computer vision application.

Although the proposed method is introduced for underwater scenes, it still can be generalized to deal with other types of degraded images. From Fig. 20, it can be seen that the proposed method can effectively improve the visibility of the sandy and hazy images.

### 5 Conclusion

In this paper, we propose an efficient method for underwater image dehazing. First, to mitigate the color distortion of the image, we design a novel color correction method, in which, selective absorption is taken into account. We then estimate the global background light from a local region of the color corrected image. Additionally, a dual transmission map strategy is used. A novel color channel with sharpened term and difference of channel intensity prior term is proposed to accurately deduce the transmission map. Finally, with the estimated background light and transmission map, the restored image is generated. Experimental results demonstrate that the proposed method achieves better natural visual quality with more valuable information and higher contrast.

Despite the excellent performance, the proposed method still introduces some limitations. It shows weak robustness to underwater images captured at the FujiFilm camera settings. In the future, we will try our best to overcome this drawback. More flexible and effective dehazing method will be proposed to enhance the complex underwater images, especially those captured in deep water.

## Appendix A

See Table 6.

**Table 6** Abbreviations used in this paper

Abbreviations	Description
IFM	image formation model
BL	background light
TM	transmission map
DCP	dark channel prior
MIP	maximum intensity prior
VE	visible edge
GPU	graphics processing unit
UGAN	underwater generative adversarial network
CycleGAN	cycle generative adversarial network
FUnIEGAN	fully-convolutional GAN-based model for underwater image enhancement
DenseGAN	dense generative adversarial network
UWCNN	underwater image enhancement convolutional neural network
RCP	red channel prior
GDCP	generalized dark channel prior
ULAP	underwater light attenuation prior
AL	artificial light
UIEBD	underwater image enhancement benchmark dataset
UIQS	underwater image quality set
PCQI	patch-based contrast quality index
UIQM	underwater image quality measures
UICM	colorfulness measure
UISM	sharpness measure
UIConM	contrast measure
UCIQE	underwater color image quality evaluation
SIFT	scale invariant feature transform

**Acknowledgements** The authors sincerely thank the editors and anonymous reviewers for the very helpful and kind comments to assist in improving the presentation of our paper. This work was supported in part by the National Natural Science Foundation of China under Grant 62176037, Grant 62002043, and Grant 61802043, by the Liaoning Revitalization Talents Program under Grant XLYC1908007, by the Foundation of Liaoning Key Research and Development Program under Grant 201801728, by the Dalian Science and Technology Innovation Fund under Grant 2018J12GX037, Grant 2019J11CY001, and Grant 2021JJ12GX028

## Declarations

**Conflict of interest** The authors declare that they have no potential conflict of interest

## References

1. Akkaynak D, Treibitz T (2018) A revised underwater image formation model. In 2018 IEEE Conf. Comput. Vis. Pattern Recognit. (CVPR), pp 6723–6732
2. Ancuti CO, Ancuti C, Vleeschouwer CD, Bekert P (2018) Color balance and fusion for underwater image enhancement. *IEEE Trans. image process* 27(1):379–393
3. Buchsbaum G (1980) A spatial processor model for object color perception. *Journal of the Franklin Institute* 310(1):337–350
4. Carlevaris-Bianco N, Mohan A, Eustice RM (2010) Initial results in underwater single image dehazing. In Oceans, IEEE
5. Chiang JY, Chen YC (2012) Underwater image enhancement by wavelength compensation and dehazing. *IEEE Trans. Image Process* 21(4):1756–1769
6. Ding X, Liang Z, Wang Y, Fu X (2021) Depth-aware total variation regularization for underwater image dehazing. *Signal Process, Image Commun.*, p 98
7. Drews-Jr P, do Nascimento ER, Moraes F, Botelho SC, Campos FM (2013) Transmission estimation in underwater single images. In IEEE Int. Conf. Comput. Vis. Workshops (ICCVW), pp 825–830
8. Fabbri C, Islam MJ, Sattar J (2018) Enhancing underwater imagery using generative adversarial networks. 2018 IEEE Int. Conf. Robot. Autom. (ICRA), pp 7159–7165
9. Fabbri C, Islam MJ, Sattar J (2018) Enhancing underwater imagery using generative adversarial networks. In 2018 IEEE Inter. Conf. Robot. Autom. (ICRA), pp 7159–7165
10. Fattal R (2008) Single image dehazing. *ACM Trans. Graph* 27(3):72
11. Finlayson GD, Trezzi E (2004) Shades of gray and colour constancy. In Color Imaging Conferenc, pp 37–41
12. Fu X, Liang Z, Ding X, Yu X, Wang Y (2020) Image descattering and absorption compensation in underwater polarimetric imaging. *Optics and Lasers in Engineering* 132
13. Fu X, Zhuang P, Huang Y, Liao Y, Zhang XP, Ding X (2014) A retinex-based enhancing approach for single underwater. 2014 IEEE Int. Conf. Image Process. (ICIP), pp 4572–4576
14. Galdran A, Pardo D, Picon A, Alvarez-Gila A (2015) Automatic red channel underwater image restoration. *J. Vis. Communun. Image Represent* 26:132–145
15. Ghani A, Isa N (2015) Enhancement of low quality underwater image through integrated global and local contrast correction. *Appl. Soft Comput* 37:332–344
16. Guo Y, Li H, Zhuang P (2020) Underwater image enhancement using a multiscale dense generative adversarial network. *IEEE J. Oceanic Engineer* 45(3):862–870
17. Hautiere N, Tarel JP, Aubert D, Dumont E (2011) Blind contrast enhancement assessment by gradient ratioing at visible edges. *Image Analysis. Stereology* 27(2):87–95
18. He K, Sun J, Tang X (2011) Single image haze removal using dark channel prior. *IEEE Trans. Pattern Anal. Mach. Intell* 33(12):2341–2353
19. He K, Sun J, Tang X (2013) Guided image filtering. *IEEE Trans. Pattern Anal. Mach. Intell* 35(6):1397–1409
20. Huang SC, Chen BH, Wang WJ (2014) Visibility restoration of single hazy images captured in real-world weather conditions. *IEEE Trans. Circuits Syst. Video Technol* 24(10):1814–1824
21. Jian M, Qi Q, Dong J, Yin Y, Lam K (2018) Integrating qdwd with pattern distinctness and local contrast for underwater saliency detection. *J. Vis. Communun. Image Represent* 53:31–41
22. Land EH (1978) The retinex theory of color vision. *Scientific American* 237(6):108–128
23. Li C, Guo J, Cong R, Pang Y, Wang B (2016) Underwater image enhancement by dehazing with minimum information loss and histogram distribution prior. *IEEE Trans. Image Process* 25(12):5664–5677

24. Li J, Skinner KA, Eustice RM, Johnson-Roberson M (2018) Watergan: Unsupervised generative network to enable real-time color correction of monocular underwater images. *IEEE Robotics Autom. Lett* 3(1):387–394
25. Li Y, Xu H, Li Y, Lu H, Serikawa S (2019) Underwater image segmentation based on fast level set method. *Int. J. Comput. Sci. Eng* 19(4):562–569
26. Li C, Guo C, Ren W, Cong R, Hou J, Kwong S, Tao D (2020) An underwater image enhancement benchmark dataset and beyond. *IEEE Trans. Image Process* 29:4376–4389
27. Li C, Anwar S, Hou J, Cong R, Guo C, Ren W (2021) Underwater image enhancement via medium transmission-guided multi-color space embedding. *IEEE Trans. Image Process* 30:4985–5000
28. Li C, Anwar S, Porikli F (2020) Underwater scene prior inspired deep underwater image and video enhancement. *Pattern Recognit* 98
29. Liu P, Yu H, Cang S (2018) Optimized adaptive tracking control for an underactuated vibro-driven capsule system. *Nonlinear Dynamics* 94(3):1803–1817
30. Liu P, Yu H, Cang S (2019) Adaptive neural network tracking control for underactuated systems with matched and mismatched disturbances. *Nonlinear Dynamics* 98(2):1447–1464
31. Liu R, Fan X, Zhu M, Hou M, Luo Z (2020) Real-world underwater enhancement: Challenges, benchmarks, and solutions under natural light. *IEEE Trans. Circuits Syst. Video Technol* 30(12):4861–4875
32. Liu X, Gao Z, Chen BM (2021) Ipmgan: Integrating physical model and generative adversarial network for underwater image enhancement. *Neurocomputing* 453:538–551
33. Lowe DG (2004) Distinctive image features from scale-invariant keypoints. *Int. J. Comput. Vis* 60(2):91–110
34. Ma X, Chen Z, Feng Z (2019) Underwater image restoration through a combination of improved dark channel prior and gray world algorithms. *J. Electronic Imaging* 28(5):053033
35. Islam MJ, Xia Y, Sattar J (2020) Fast underwater image enhancement for improved visual perception. *IEEE Robotics Autom. Lett* 5(2):3227–3234
36. Narasimhan SG, Nayar SK (2000) Chromatic framework for vision in bad weather. In: *IEEE Conf. Comput. Vis. Pattern Recognit. (CVPR)*, pp 1598–1605
37. Panetta K, Gao C, Agaian S (2016) Human-visual-system-inspired underwater image quality measures. *IEEE J. Oceanic Engineer* 41(3):541–551
38. Peng Y-T, Cao K, Cosman PC (2018) Generalization of the dark channel prior for single image restoration. *IEEE Trans. Image Process* 27(6):2856–2868
39. Sahu G, Seal A, Krejcar O, Yazidi A (2021) Single image dehazing using a new color channel. *J. Vis. Communun, Image Represent*, p 74
40. Sharma G, Wu W, Dalal EN (2005) The ciede2000 color-difference formula: Implementation notes, supplementary test data, and mathematical observations. *Color Research Application* 30(1):21–30
41. Shen J, Robertson N (2021) Bbas: Towards large scale effective ensemble adversarial attacks against deep neural network learning. *Inf. Sci* 569:469–478
42. Song W, Wang Y, Huang DM, Tjondronegoro D (2018) A rapid scene depth estimation model based on underwater light attenuation prior for underwater image restoration. *Advances in Multimedia Information Processing - PCM* 2018:678–688
43. Sun L, Zhao C, Yan Z, Liu P, Duckett T, Stolk R (2018) A novel weakly-supervised approach for rgb-d-based nuclear waste object detection and categorization. *IEEE Sensors Journal* 19(9):3487–3500
44. Tang K, Yang J, Wang J (2014) Investigating haze-relevant features in a learning framework for image dehazing. In: *Computer Vision Pattern Recognition*, pp 2995–3002
45. Ulutas G, Ustubioglu B (2021) Underwater image enhancement using contrast limited adaptive histogram equalization and layered difference representation. *Multim. Tools Appl* 80(10):15067–15091
46. Wang S, Ma K, Yeganeh H, Wang Z, Lin W (2015) A patch-structure representation method for quality assessment of contrast changed images. *IEEE Signal Process. Lett* 22(12):2387–2390
47. Wang Y, Wang H, Yin C, Dai M (2016) Biologically inspired image enhancement based on retinex. *Neurocomputing* 177:373–384
48. Wang L, Qian X, Zhang Y, Shen J, Cao X (2020) Enhancing sketch-based image retrieval by cnn semantic re-ranking. *IEEE Trans. Cybern* 50(7):3330–3342
49. Wang Z, She Q, Ward TE (2021) Generative adversarial networks in computer vision: A survey and taxonomy. *ACM Comput. Surv* 54(2):1–38
50. Wang Y, Liu H, Chau LP (2018) Single underwater image restoration using adaptive attenuation-curve prior. *IEEE Trans. Circuits Syst. I Regul. Pap* 65-I(3):992–1002
51. Wei X, Lu W, Xing W (2017) A rapid multi-source shortest path algorithm for interactive image segmentation. *Multim. Tools Appl* 76(20):21547–21563
52. Weijer JVD, Gevers T, Gijsenij A (2007) Edge-based color constancy. *IEEE Trans. Image Process* 16(9):2207–2214

53. Yan X, Wang G, Jiang G, Wang Y, Mi Z, Fu X (2022) A natural-based fusion strategy for underwater image enhancement. *Tools Appl, Multim.* <https://doi.org/10.1007/s11042-022-12267-7>
54. Yan X, Wang G, Wang G, Wang Y, Fu X (2022) A novel biologically-inspired method for underwater image enhancement. *Signal Process. Image Commun* 104:116670. <https://doi.org/10.1016/j.image.2022.116670>
55. Yang KF, Gao SB, Li YJ (2015) Efficient illuminant estimation for color constancy using grey pixels. In: 2015 IEEE Conf. Comput. Vis. Pattern Recognit. (CVPR), pp 2254–2263
56. Yang M, Sowmya A (2015) An underwater color image quality evaluation metric. *IEEE Trans. Image Process* 24(12):6062–6071
57. Yu H, Li X, Lou Q, Lei C, Liu Z (2020) Underwater image enhancement based on dcp and depth transmission map. *Multim. Tools Appl* 79(27–28):20373–20390
58. Yuan F, Zhan L, Pan P, Cheng E (2021) Low bit-rate compression of underwater image based on human visual system. *Signal Process, Image Commun*, p 91
59. Zhang W, Dong L, Zhang T, Xu W (2021) Enhancing underwater image via color correction and bi-interval contrast enhancement. *Signal Process, Image Commun*, p 90
60. Zhang W, Liu W, Li L, Li J, Zhang M, Li Y (2021) An adaptive color correction method for underwater single image haze removal. *Signal Image Video Process*
61. Zhu JY, Park T, Isola P, Efros AA (2017) Unpaired image-to-image translation using cycle-consistent adversarial networks. *IEEE International Conference on Computer Vision (ICCV)*, pp 2242–2251
62. Zhu Q, Mai J, Shao L (2015) A fast single image haze removal algorithm using color attenuation prior. *IEEE Trans. Image Process* 24(11):3522–3533
63. Zhuang P, Ding X (2020) Underwater image enhancement using an edge-preserving filtering retinex algorithm. *Multim. Tools Appl* 79(25–26):17257–17277

**Publisher's Note** Springer Nature remains neutral with regard to jurisdictional claims in published maps and institutional affiliations.

Springer Nature or its licensor (e.g. a society or other partner) holds exclusive rights to this article under a publishing agreement with the author(s) or other rightsholder(s); author self-archiving of the accepted manuscript version of this article is solely governed by the terms of such publishing agreement and applicable law.

## Terms and Conditions

Springer Nature journal content, brought to you courtesy of Springer Nature Customer Service Center GmbH (“Springer Nature”).

Springer Nature supports a reasonable amount of sharing of research papers by authors, subscribers and authorised users (“Users”), for small-scale personal, non-commercial use provided that all copyright, trade and service marks and other proprietary notices are maintained. By accessing, sharing, receiving or otherwise using the Springer Nature journal content you agree to these terms of use (“Terms”). For these purposes, Springer Nature considers academic use (by researchers and students) to be non-commercial.

These Terms are supplementary and will apply in addition to any applicable website terms and conditions, a relevant site licence or a personal subscription. These Terms will prevail over any conflict or ambiguity with regards to the relevant terms, a site licence or a personal subscription (to the extent of the conflict or ambiguity only). For Creative Commons-licensed articles, the terms of the Creative Commons license used will apply.

We collect and use personal data to provide access to the Springer Nature journal content. We may also use these personal data internally within ResearchGate and Springer Nature and as agreed share it, in an anonymised way, for purposes of tracking, analysis and reporting. We will not otherwise disclose your personal data outside the ResearchGate or the Springer Nature group of companies unless we have your permission as detailed in the Privacy Policy.

While Users may use the Springer Nature journal content for small scale, personal non-commercial use, it is important to note that Users may not:

1. use such content for the purpose of providing other users with access on a regular or large scale basis or as a means to circumvent access control;
2. use such content where to do so would be considered a criminal or statutory offence in any jurisdiction, or gives rise to civil liability, or is otherwise unlawful;
3. falsely or misleadingly imply or suggest endorsement, approval , sponsorship, or association unless explicitly agreed to by Springer Nature in writing;
4. use bots or other automated methods to access the content or redirect messages
5. override any security feature or exclusionary protocol; or
6. share the content in order to create substitute for Springer Nature products or services or a systematic database of Springer Nature journal content.

In line with the restriction against commercial use, Springer Nature does not permit the creation of a product or service that creates revenue, royalties, rent or income from our content or its inclusion as part of a paid for service or for other commercial gain. Springer Nature journal content cannot be used for inter-library loans and librarians may not upload Springer Nature journal content on a large scale into their, or any other, institutional repository.

These terms of use are reviewed regularly and may be amended at any time. Springer Nature is not obligated to publish any information or content on this website and may remove it or features or functionality at our sole discretion, at any time with or without notice. Springer Nature may revoke this licence to you at any time and remove access to any copies of the Springer Nature journal content which have been saved.

To the fullest extent permitted by law, Springer Nature makes no warranties, representations or guarantees to Users, either express or implied with respect to the Springer nature journal content and all parties disclaim and waive any implied warranties or warranties imposed by law, including merchantability or fitness for any particular purpose.

Please note that these rights do not automatically extend to content, data or other material published by Springer Nature that may be licensed from third parties.

If you would like to use or distribute our Springer Nature journal content to a wider audience or on a regular basis or in any other manner not expressly permitted by these Terms, please contact Springer Nature at

[onlineservice@springernature.com](mailto:onlineservice@springernature.com)